Chamberlain, K.J., Barclay, J., Preece, K., Brown, R.J., and Davidson, J.P. (2016) Origin and evolution of silicic magmas at ocean islands: Perspectives from a zoned fall deposit on Ascension Island, South Atlantic. Journal of Volcanology and Geothermal Research, 327, 349 - 360.

http://eprints.gla.ac.uk/136341/

Deposited on: 8 February 2017

1   Origin and evolution of silicic magmas at ocean islands: Perspectives

2   from a zoned fall deposit on Ascension Island, South Atlantic

3

4

5

6

7

8 **K. J. CHAMBERLAIN[1*], J. BARCLAY[2], K. PREECE[2], R. J. BROWN[1], J. P. DAVIDSON[1],**

9 **EIMF[3]**

10

11

12

13

14 [1] DEPARTMENT OF EARTH SCIENCES, UNIVERSITY OF DURHAM, DURHAM, DH1 3LE, UK

15 [2] SCHOOL OF ENVIRONMENTAL SCIENCES, UNIVERSITY OF EAST ANGLIA, NORWICH, NR4 7TJ, UK

16 [3] EDINBURGH ION MICROPROBE FACILITY, UNIVERSITY OF EDINBURGH, EDINBURGH,

17

18

19

20

21

22

23

24

25

26

34

35 *Corresponding author. Phone (+44) 191 334 2300, Fax (+44) 191 334 2301
36 Email addresses: katyjanechamberlain@gmail.com

37

1 **ABSTRACT**

2 Ascension Island, in the south Atlantic is a composite ocean island volcano with a wide

3 variety of eruptive styles and magmatic compositions evident in its ~1 million year subaerial

4 history. In this paper, new observations of a unique zoned fall deposit on the island are

5 presented; the deposit gradationally changes from trachytic pumice at the base, through to

6 trachy-basaltic andesite at the top of the deposit. The key features of the eruptive deposits are

7 described and are coupled with whole rock XRF data, major and trace element analyses of

8 phenocrysts, groundmass glass and melt inclusions from samples of the compositionally-

9 zoned fall deposit to analyse the processes leading up to and driving the explosive eruption.

10 Closed system crystal fractionation is the dominant control on compositional zonation, with

11 the fractionating assemblage dominated by plagioclase feldspar and olivine. This

12 fractionation from the trachy-basaltic andesite magma occurred at pressures of ~ 250 MPa.

13 There is no evidence for multiple stages of evolution involving changing magmatic

14 conditions or the addition of new magmatic pulses preserved within the crystal cargo.

15 Volatile concentrations range from 0.5 to 4.0 wt.% H_2O and progressively increase in the

16 more evolved units, suggesting crystal fractionation concentrated volatiles into the melt

17 phase, eventually causing internal overpressure of the system and eruption of the single

18 compositionally-zoned magma body. Melt inclusion data combined with Fe–Ti oxide

19 modelling suggests that the oxygen fugacity of Ascension Island magmas is not affected by

20 degree of evolution, which concentrates H_2O into the liquid phase, and thus the two systems

21 are decoupled on Ascension, similar to that observed in Iceland. This detailed study of the

22 zoned fall deposit on Ascension Island highlights the relatively closed-system evolution of

23 felsic magmas at Ascension Island, in contrast to many other ocean islands, such as Tenerife

24 and Iceland.

25

26 **INTRODUCTION**

27 Ascension Island, in the south Atlantic, is a 12 km diameter ocean island volcano

28 located 90 km west of the mid Atlantic Ridge (MAR). It is similar to Iceland and many other

29 ocean island volcanoes in having a significant proportion of silicic volcanic products

30 preserved at the surface (~14% of the surface exposure, Nielson & Sibbett, 1996, compared

31 with ~10% surface area in Iceland, Walker, 1966, Carley et al., 2011). Understanding the

32 processes responsible for the production of silicic magmas at ocean islands is important not

33 only for our present understanding of magmatic processes and magmatic evolution, but also

34 provides critical insights into the mechanisms behind the generation of the first continental

1 crust in the Archean (e.g. Gazel et al., 2014; Mancini et al., 2015). Two main methods have
2 been proposed for the generation of evolved melts in thin oceanic crust: (i) low-degree
3 partial melting of hydrothermally-altered crust to produce primary silicic melt (e.g.
4 Sverrisdottir, 2007; Carley et al., 2011; Kuritani et al., 2011) or (ii) fractionation (in
5 potentially multiple stages) from a basaltic parental magma (e.g. Watanabe et al., 2006;
6 Snyder et al., 2007; Mortensen et al., 2009; Mancini et al., 2015), or some combination of
7 these processes.

8   Zoned volcanic deposits preserve the moment in magmatic evolution when distinct
9 magmas are erupted together, and might only be observable through disequilibria in
10 phenocryst assemblages in otherwise homogeneous deposits. They can provide a direct
11 record of processes responsible for magmatic evolution (and timescales over which they
12 occur), such as fractionation, mixing and assimilation (e.g. Watanabe et al., 2006; Snyder et
13 al., 2007; Sverrisdottir, 2007; Mortensen et al., 2009; Carley et al., 2011; Kuritani et al.,
14 2011; Mancini et al., 2015).

15   Zoned volcanic deposits may also yield insights into the processes responsible for
16 eruptive triggering (e.g. Sverrisdottir, 2007; Kuritani et al., 2011). Recharge of volcanic
17 systems (potentially preserved as two magmatic types in zoned volcanic deposits) has often
18 been cited as a trigger for eruptions (e.g. Sparks and Sigurdsson 1977; Pallister et al., 1992;
19 Sverisdottir, 2007; Saunders et al., 2012; Sliwinski et al., 2015) whether due to a direct
20 increase in volume, causing failure of the magma chamber wall rocks (e.g. Jellinek and
21 DePaolo 2003), the buoyancy-driven effects of accumulating magma (e.g. Carrichi et al.,
22 2014; Malfait et al., 2014), or by indirectly causing changes in volume of saturated gases and
23 crystal cargo (e.g. Snyder 2000). However, other eruptive triggers are well-documented,
24 including tectonic triggers from earthquake activity (e.g. Allan et al., 2012), changing crustal
25 stress-states (e.g. Bonali et al., 2013) and internal overpressure from crystal fractionation
26 driving increased volatile concentrations in the remaining magma (e.g. Stock et al., 2016).

27   Here we present field observations, whole rock major and trace element data, mineral
28 compositions and melt inclusion analyses from a unique zoned fall deposit on Ascension
29 Island, to understand the processes responsible for silicic melt generation, evolution and
30 eruption in young (<7 Ma) oceanic crust on Ascension Island. The zoned fall deposit is
31 unique on Ascension Island in that it changes gradationally from trachytic pumice at the base
32 of the unit, to a trachy-basaltic andesite scoria at the top of the unit, with no textural evidence
33 for mingling between pumice and scoria. We use this deposit to probe the origins of felsic
34 melt at Ascension Island, to understand how the zonation is produced, and by inference what

1   may have triggered the eruption. In particular, we use this deposit to test whether the zonation

2   is the result of two distinct magma batches partially homogenizing (open system), if it is

3   generated via *in situ* fractionation (closed system), or if it is the result of a combination of

4   multiple processes.

5

6   **GEOLOGICAL SETTING**

7   Ascension Island (7° 56' S; 14° 22' W) is located in the southern Atlantic Ocean, 90 km west

8   of the Mid-Atlantic Ridge and 50 km south of the Ascension Fracture Zone (AFZ; Fig. 1).

9   Volcanism has been present at Ascension for ~ 6 – 7 Myr and the subaerial portion of the

10   island (only 1% of the total ~3800 km^3 edifice, Harris, 1983) was formed in the last ~1 Myr

11   (Weaver et al., 1996; Jicha et al., 2014). Volcanic deposits on Ascension are widely variable,

12   with lava flows, lava domes, pyroclastic fall units, pyroclastic flow units (Daly, 1925; Harris,

13   1983; Weaver et al., 1996; Hobson, 2001).

14   Subaerial volcanism has been the product of a transitional to mildly alkali magmatic

15   series of olivine basalt – hawaiite – mugearite – benmoreite – trachyte – rhyolite. Previous

16   investigations into Ascension Island volcanism have focussed on the geochemical distinctions

17   between magmas; mafic volcanic products have been split into three main categories, based

18   on their Zr/Nb ratios, which has been inferred to represent varying source characteristics

19   underlying Ascension. Mafic volcanic products occur across all of Ascension, but felsic

20   volcanic products are more localised and outcrop in two main areas of the island: a 'Central

21   Felsic Complex', which contains Green Mountain, the highest point on the island at 859m

22   asl, (see Fig. 1; Kar et al., 1998) and the younger 'Eastern Felsic Complex' (Fig. 1; Kar et al.,

23   1998; Hobson, 2001; Jicha et al., 2014). Previous studies have suggested that the felsic

24   magmas are a product of fractional crystallisation from the high Zr/Nb basalt (Weaver et al.,

25   1996; Kar et al., 1998), with limited evidence for interaction between magma batches (Kar et

26   al., 1998).

27

28   **THE COMPOSITIONALLY ZONED FALL**

29   The compositionally-zoned fall unit (Fig. 2) is found in multiple locations across the island

30   (Fig. 3) although it is dominantly found in the Eastern Complex (Fig. 1). Along the North

31   East coast the compositionally-zoned fall outcrops below a (geochemically un-related)

32   voluminous trachyte flow at NE Bay, which has a ^{40}Ar/^{39}Ar date of 169 ka (±43 ka [2σ],

33   Jicha et al., 2014). Thus the eruption responsible for the deposition of the compositionally-

34   zoned fall is also likely comparatively young.

1　　　　The vent for the compositionally-zoned fall deposit was identified by the coarsening

2　characteristics of the multiple exposures (see Fig. 3 for maximum lithic clast and thickness

3　variations at every outcrop observed), and by the presence of a fissure through an underlying

4　mafic lava flow, overlain by the coarsest and thickest deposits of the compositionally-zoned

5　fall on the island. At this locality the bombs of pumice are up to 30 cm in diameter, and lithic

6　clasts (of trachyte lava and dense mafic lava and scoria) are up to 15 cm in diameter. The

7　limited outcrops indicate dispersal towards the north east, which is consistent with the

8　dominant south-westerly wind direction at Ascension (see Fig. 3).

9　　　　For the purposes of systematic sampling, three distinct subunits were delineated (Figs.

10　2, 3). The lowermost subunit (A) consists of felsic cream to light brown coloured pumice

11　which is variably oxidised to orange and purple colours in the centre of clasts, and ~15%

12　lithic clasts. Juvenile pumice is crystal poor, with <5% crystals which include feldspar and

13　olivine. Crystals are always <1 mm in diameter. Lithic clasts present include green trachyte

14　lava and mafic lava (oxidised to red and unoxidised black). Subunit B marks the first

15　appearance of the transitional brown pumice-scoria with a coarser vesicularity than that of the

16　light brown pumice (Fig. 4). The change from cream pumice to brown pumice-scoria is

17　gradational, with transitional light brown pumice-scoria clasts identified, implying that the

18　change in colour is both textural and compositional in origin. Lithic clasts comprise ~15% of

19　this unit, and are dense mafic lavas (red and black) and minor green trachyte lavas. Juvenile

20　pumice-scoria is crystal poor with <5% macrocrysts, and feldspar is the only identifiable

21　phase in hand sample. Subunit C marks the change to less than 15% pumice in the unit

22　(gradational), and the juvenile material is dominated by dark brown scoriacious clasts. Lithic

23　clasts are now ~10% and consist of dense mafic lavas (oxidised and unoxidised). The scoria

24　has a very coarse vesicularity, with vesicles up to cm-scale (Fig. 4).

25　　　　The compositionally-zoned fall deposit is most easily recognised by the systematic

26　zonation of cream pumice clasts (subunit A) passing upwards into brown pumice-scoria

27　(subunit B) to dark brown scoria (subunit C; Fig. 2). The compositionally-zoned fall unit

28　varies in thickness from ~50 cm in the central areas of the island, to more than 10 m adjacent

29　to the vent (see Fig. 3). The deposit generally has a fine-grained base, which coarsens

30　upwards to the centre of the subunit A (Fig. 2), with the coarsest juvenile clasts in the

31　lowermost 20-50% of subunit A (Fig. 2), indicating that the eruption reached its maximum

32　energy output prior to the eruption of less-evolved magma.

33

34　**SAMPLING AND ANALYTICAL TECHNIQUES**

1   Bulk samples were collected from the three subunits of the zoned fall deposit (Fig. 2).

2   Samples were sieved to >8mm or >16mm to ensure than any lithic clasts could be identified

3   and removed by hand. Samples were collected from multiple localities and analysed for

4   whole rock major and trace elements (Fig. 3). One locality (Fig. 3) was sampled more

5   intensively than the three major subunits to understand in more details the nature of the

6   zonation in the fall deposit (see Table 1 for sampling details).

7   Any adhering matrix or oxidised rind was removed by hand, and samples were then

8   soaked in (frequently changed) milli-RO water for a minimum of one week. Samples were

9   then dried thoroughly at 60 °C prior to crushing. An aliquot of the sample was selected to

10 mill for X-ray fluorescence (XRF) analysis at the University of East Anglia (UEA) using a

11 Brucker-AXS S4 Pioneer. The remainder of the sample was crushed by hand, before being

12 sieved into various size fractions (< 2 mm). Crystals and glass separates were hand-picked

13 from the 0.5 – 1 mm size fraction, mounted into low-activity epoxy discs, and polished to

14 expose melt inclusions and crystal cores. Melt inclusion-bearing crystals were imaged using

15 reflected light microscopy prior to analysis. Secondary ion mass spectrometry (SIMS)

16 measurements of selected volatile and trace elements were made prior to measurement of

17 other major and trace elements by electron probe microanalysis (EPMA) and laser ablation

18 inductively coupled plasma mass spectrometry (LA-ICPMS), following the method of

19 Humphreys et al. (2006).

20   Mounts of melt-inclusion bearing crystals were gold-coated and analysed using

21 secondary ion mass spectrometry (SIMS) for isotopes of volatile ($^1H^+$ and $^{12}C^+$) and key trace

22 elements (Li, B, Be, F, S, Cl, Rb, Sr, Zr, Nb, Ba) using a Cameca 1270 ion microprobe at the

23 NERC Ion Microprobe Facility at the University of Edinburgh (UK). During analysis, the

24 primary beam was rastered for 180 seconds over an area of about 35 μm^2 prior to data

25 acquisition to remove the gold coat and any possible surface contamination. Secondary ions

26 were then sputtered from melt inclusions with a 5-6 nA primary $^{16}O_2^-$ beam focused to a

27 ~25×35 μm spot. The area analysed was reduced using a (field) aperture to accept on the

28 central 20 μm^2 of the bombarded area. Analyses were done in two parts; initially volatiles H,

29 C, F, S, and Cl (plus majors Mg^{2+} and Si) followed by traces Li, Be, B, Rb, Sr, Zr, Nb and Ba

30 (plus majors Mg and Si) in the same hole. Energy filtering (75±20 eV) was employed to

31 reduce the molecular ion presence, the ratio susceptibility to charging effects and any

32 potential matrix effects.   The mass resolution employed (M/ΔM>2500) was sufficient to

33 fully resolve $^{12}C^+$ from $^{24}Mg^{2+}$, $^{32}S^+$ from $^{16}O_2^+$ etc.

1   *In-situ* major element analyses were obtained by EPMA using a JEOL JXA 8230

2   system at Victoria University of Wellington (VUW), or using a CAMECA SX100 at the

3   University of Edinburgh, both using wavelength-dispersive spectrometry. Precision of

4   standard analyses of major elements (>5 wt.% concentration) is always within 2 relative % (2

5   s.d.); uncertainties are slightly higher for minor elements. Due to their hydrated nature only

6   glass analyses with totals of <93 wt.% were set aside; values for the remaining analyses were

7   then normalised to 100 %. Prior to analysis, back-scattered electron (BSE) images were taken

8   of all melt inclusions and crystal phases to identify zoning patterns and locate analytical

9   spots. This was carried out VUW using the EPMA, and at UEA using a JEOL JSM 5900LV

10   scanning electron microscope (SEM).

11   Trace element analyses of crystal phases and matrix glass were carried out at the

12   University of Durham using New Wave deep UV laser (193 nm solid state) coupled to an X-

13   series 2 ICPMS. Analyses were run using a 35 μm spot. The LA-ICPMS data were internally

14   normalized to ^{29}Si or ^{43}Ca from EPMA analyses. Abundances of single trace elements were

15   calculated relative to a bracketing standard (NIST 612) which was analysed throughout the

16   run under identical conditions. Precision and accuracies varied depending on the analytical

17   conditions but generally have <10% (2 s.d.) uncertainties (see Electronic Appendix).

18

19   **RESULTS**

20   *Whole rock major and trace elements*

21   XRF analyses of samples taken at seven intervals through the fall deposit (for sampling

22   interval details see Table 1; full results in electronic appendix) were analysed to complement

23   the detailed crystal and glass analyses from the three identified subunits (see below).

24   Systematic changes in most major and trace elements analysed are evident, with the upper-

25   most sample of trachy-basaltic andesite (i.e. the top of subunit C) being enriched in MgO,

26   Fe_2O_3, CaO, TiO_2, P_2O_5, V and Sr relative to all stratigraphically-lower samples (Fig. 5). In

27   contrast, the lower-most trachytic sample is enriched in SiO_2, K_2O, Na_2O, Rb, Zr, Nb, Ba, La,

28   Ce (Fig. 5) relative to all stratigraphically-higher samples, while there is no measureable

29   change in MnO, Al_2O_3, Ni, Cu, Cr, ZN, Y, Pb, Th or U throughout the deposit.

30

31   *Petrography*

32   The zoned fall is a crystal-poor deposit, with less than 5% crystals (by volume). The

33   dominant crystal phases (in decreasing order of abundance) are plagioclase feldspar + olivine

34   ± anorthoclase feldspar + ilmenite + magnetite, and all are < 0.5mm in diameter. Rare

1   accessory phases of apatite and allanite are occasionally present. Clinopyroxene is present

2   only in the upper, more mafic compositions. BSE images of the two feldspars, olivine,

3   clinopyroxene and Fe–Ti oxides show no visible zoning, and all crystal phases are euhedral

4   (Fig. 6). Olivine is typically melt inclusion –rich, with multiple melt inclusions per crystal

5   and melt inclusions are occasionally linked to the exterior of the crystal, giving an embayed

6   appearance (Fig. 6a, b). However, there is no evidence in any other crystal phases for any

7   dissolution having occurred.

8

9   *Phenocryst compositions*

10   Major and trace element analyses of feldspars were carried out on samples from the three

11   subunits of the zoned fall. Two populations of feldspars are identified (Fig. 7a) - a sanidine-

12   anorthoclase component ($An_2Or_{38}Ab_{60}$), and an andesine component ($An_{40}Or_2Ab_{58}$). There is

13   no systematic difference between core and rim analyses in any subunit sample, and neither

14   feldspar populations have any observable zonation visible in BSE imagery (Fig. 6). Similarly,

15   crystal habits are euhedral, with no textural evidence for textural disequilibrium between the

16   melt and the two feldspar groups. Feldspars from the three subunits are overlapping in their

17   feldspar compositions with no major variations apparent, however feldspars from subunits B

18   and C have slightly higher Sr concentrations at lower silica concentrations than feldspars

19   from subunit A (Fig. 7a).

20   Major and trace element analyses of olivine crystals show a range in compositions

21   from Fo_{45} to Fo_8 (Fig. 7b). Similar to the feldspar, the olivine shows no systematic variation

22   between cores and rims, or within subgroups. While all three subunits have overlapping

23   olivine compositions, subunits B and C extend to slightly higher forsterite compositions at

24   lower MnO concentrations (Fig. 7b).

25

26   *Matrix glass and melt inclusions*

27   Major and trace element analyses of melt inclusions and matrix glass are overlapping, and

28   span a range of ~55 wt.% SiO_2 to ~70 wt.% SiO_2 (Fig. 8). Glass analyses of major and trace

29   elements show a systematic difference between subunits, with subunit A being the most-

30   evolved (SiO_2 63 – 70 wt.%), subunit B being transitional (SiO_2 59 – 66 wt.%), and subunit C

31   having the least-evolved glass compositions (SiO_2 55 – 63 wt.%; Fig. 8a). Subunit A is also

32   enriched in K_2O, Na_2O, Rb, Zr, Ba, the light rare earth elements (LREE) and Pb, whilst being

33   depleted in TiO_2, FeO, MgO, CaO, P_2O_5, Sr and Eu relative to subunit C (see Fig. 8 and

34   Electronic Appendix).

1   SEM images of melt inclusions reveal many inclusions that are not fully entrapped

2   (Fig. 6), with the potential that some inclusions whilst appearing isolated in 2 dimensions

3   may be connected to an exterior surface in three dimensions. While care was taken to analyse

4   only fully enclosed inclusions, some results show clear influence of post-entrapment

5   degassing (Fig. 8). Volatile concentrations measured in the melt inclusions are variably

6   degassed, and therefore do not reflect primary volatile concentrations (Fig. 8c, d). However,

7   un-degassed melt inclusions from all subunits show H_2O concentrations between 2 and 4

8   wt.%, and show a weak negative correlation with key trace elements sensitive to fractional

9   crystallisation such as Sr and Eu (Fig. 8c, d). CO_2 concentrations are up to 1000 ppm (Fig.

10   8c). Concentrations of halogens in un-degassed melt inclusions do not show any discernible

11   differences between the identified subunits, and do not correlate with any measured trace

12   element (see Electronic Appendix).

13

14   **MAGMATIC CONDITIONS**

15   *Temperature & fO_2*

16   EPMA analyses of coexisting Fe–Ti oxides were undertaken, and tested for equilibrium using

17   the calculations of Bacon & Hirschman (1988). All pairs that were within the allowable

18   bounds were then used to model equilibrium temperatures and oxygen fugacities of the

19   coexisting Fe–Ti oxides, using the calibrations of Ghiorso & Evans (2008). Results are

20   displayed in Table 2. Oxides from subunit A yield an average model temperature of 845 °C

21   with an oxygen fugacity of -2.28 log units relative to the Nickel- Nickel Oxide (NNO) buffer.

22   In subunit C, average modelled temperatures are 866 °C, and fO_2 of -1.94 log units ΔNNO.

23   Given the commonly cited uncertainties of ± 30 °C associated with Fe–Ti oxide thermometry

24   (e.g. Blundy & Cashman, 2008) these results indicate limited resolvable differences in

25   temperature between the samples of the zoned fall. Hence, there is little evidence for a

26   thermal gradient existing within the magmatic system in the months to weeks prior to

27   eruption.

28   The highly reducing fO_2 of the system is surprising given the high H_2O concentrations

29   measured in melt inclusions (Fig. 8; Electronic Appendix), given that it is normally inferred

30   that the fO_2 and H_2O systematics are coupled (Lee et al., 2005). However, the calculated

31   oxygen fugacities are in line with the observed mineralogy (fayalite-rich) and the tectonic

32   (ocean island) setting (Carmichael, 1991). It is not thought that fO_2 is affected by

33   fractionation processes, and therefore can maintain the relatively reduced nature of the

34   magma, whilst H_2O proportions are systematically increasing due to its generally

1   incompatible behaviour in the fractionating phases (Carmichael, 1991; Portnyagin et al.,

2   2012). Thus, we see evidence for decoupling of the H_2O and fO_2 systematic at Ascension

3   Island, similar to that suggested at Hekla volcano, Iceland (Portnyagin et al., 2012).

4

5   *Pressure*

6   Entrapment pressures for the measured melt inclusions were calculated using the MagmaSat

7   application developed from Gualda & Ghiorso (2014) which takes into account not only the

8   measured volatile concentrations, but also the major element composition of the host melt

9   inclusion. A single temperature of 850 °C, based on our Fe–Ti oxide thermometry, was used

10   to calculate entrapment pressures. Given the potentially 'leaky' morphology of our olivine-

11   hosted melt inclusions (Fig. 6) in 3D, the maximum entrapment pressures for each unit were

12   taken as the true entrapment pressures (Table 2), but the range in modelled pressures clearly

13   shows the effect of some partial degassing of the inclusions during ascent of the magmas

14   (Fig. 9). There is no systematic difference in entrapment pressures between all three subunits

15   of the zoned fall. These entrapment pressures of ~250 MPa correspond to a depth of ~8.5 km

16   (assuming a crustal density of 3000 kg/m^3); the base of the oceanic crust at Ascension

17   (Klingelhöfer et al., 2001). It is important to note that these modelled entrapment pressures

18   only represent the pressure at which crystal were growing and trapping melt inclusions, and

19   there is no record preserved of any magmatic evolution (and the depths at which that

20   occurred) prior to crystal growth.

21

22   **DISCUSSION**

23   The gradationally zoned fall deposit, zoned in composition but not temperature, is a unique

24   deposit on Ascension Island. Here we discuss the nature of the stratification, causes for the

25   stratification within the magma chamber, eruption triggering mechanisms and how

26   representative these processes are for all evolved magmatism on Ascension Island.

27

28   *Evolution of the zoned fall*

29   The modelled entrapment pressures from melt inclusions within crystal cores compared with

30   those trapped in crystal rims, are overlapping. We thus consider that the crystals grew within

31   a stalled body of magma, rather than representing crystal growth and melt inclusion

32   entrapment upon ascent. Thus, we use melt inclusion and matrix glass compositions to look at

33   the evolutionary processes occurring within the melt dominant magma body prior to eruption.

34   We first consider the nature of the final stratification of the zoned fall magma body:

　Final stratification

2　There are two potential causes for the gradational stratification preserved in the whole rock

3　and matrix glass chemistry (Figs. 5, 8a); either two compositionally distinct magmas

4　interacted, mixed and homogenised (i.e. in an open-system); or a single magma batch stalled

5　and evolved (i.e. in a closed-system). If the first case occurred we would expect to see

6　bimodality in both phenocryst and trapped melt inclusion compositions, potentially with

7　some evidence for disequilibrium textures within the crystal cargo. However, as previously

8　shown, all crystals appear to be in equilibrium with the melt in which they were erupted (Fig.

9　6): there is no evidence for chemical changes recorded within crystal interiors (cf. Morgan et

10　al., 2004; Sliwinski et al., 2015). Furthermore while melt inclusion entrapment pressures

11　could represent re-homogenization of melt inclusions at a stalling point, this appears unlikely

12　given that melt inclusion compositions are very similar to those of matrix glasses (Fig. 8a).

13　The overlap in entrapment pressures from all units, lack of zonation within crystals, and

14　overlapping melt inclusion and matrix glass compositions shows that no magma mixing,

15　prior to crystal growth in the melt dominant body, has occurred, and yet the chemical

16　zonation remains. Therefore the compositional zonation sampled by the zoned fall deposit on

17　Ascension Island appears to have been generated by closed-system evolution in a single

18　magma chamber.

19

20　Role of fractional crystallisation

21　In order to assess the role of fractional crystallisation in generating the zoned fall deposit, we

22　applied the least-squares modelling technique of Stormer and Nichols (1978) though the

23　PetroGraph model of Petrelli et al. (2005) to the major element compositions. Whole rock

24　compositions of subunit C (i.e. the least-evolved; Fig. 5) are used as our starting

25　compositions. Fractionating phase compositions are modelled from our EPMA analyses of

26　crystal phases present in subunit C (see Electronic Appendix). However, apatite (which is

27　present as a minor component in many Ascension Island rocks, Kar et al., 1998) was not

28　directly measured, so an average composition was taken from Stock et al. (2016). The results

29　of this fractionation modelling (where the sum of the residuals is < 0.12) reveals that the

30　least-evolved magma composition can be directly related to the magma composition of

31　subunit A (i.e. the most-evolved; Fig. 5) by simple crystal fractionation, dominated by

32　plagioclase feldspar (61.6%) and olivine (22.5%) (mirroring the dominant crystal phases, see

33　results). Fractionation of minor amounts of Fe–Ti oxides (6.3%), clinopyroxene (5.7%) and

34　apatite (3.9%) also contribute to the evolution of least- to most-evolved magma compositions

in the zoned fall deposit. Interestingly, this modelling also suggests that the unzoned sanidine-anorthoclase feldspar (see results) is an accumulated, rather than fractionated phase, although the role this plays in developing the zonation within the zoned fall is minor. These more-evolved anorthoclase feldspars are likely to be sourced from surrounding plutonic bodies (studied by Harris, 1983; Kar et al., 1998; Webster & Rebbert, 2001) which are present in the surrounding crust, and often appear as lithic clasts within many fall deposits on Ascension Island (Hobson, 2001).

The lack of significant open-system behaviour in the generation of the zoned fall deposit on Ascension Island contrasts with many other ocean island volcanoes such as Iceland and Tenerife, where there is significant evidence for magma mixing and crustal assimilation (e.g. Ablay et al., 1998; Sverisdottir, 2007; Carley et al., 2011; Kuritani et al., 2011; Wiesmaier et al., 2013). Currently, there is no geothermal activity present on Ascension Island, with heat flow measurements ranging from 75 to 124 mW/m^2 (Nielson et al., 1996) in shallow (< 600 m) boreholes drilled on the island. This is much lower than other ocean islands where geothermal power plants exploit the high heat flows from magmatism (e.g. Iceland) but whether this is representative of the entirety of Ascension's volcanic history, or if reflects a potential cessation of volcanism at Ascension is not known. However, given the relatively slow volcanic growth rates modelled by Minshull et al. (2010) of 0.4 km/Myr (compared with average growth rates of 4.6 km/Myr of Mauna Kea during both its shield building stage, and post-shield stage; Sharp & Renne, 2005), it would seem that rates of magma flux during Ascension's volcanic history have been low, and thus favour closed-system evolution with limited magma mixing.

Convection in a stratified magma body?

The detailed field data show that the zoned fall deposit was erupted from a single vent source. Further to this, the geochemical analyses, reveal a systematic gradation (e.g. Figs. 5 – 8), and therefore confirm that the deposit is the result of the evacuation of a single zoned magma body. In order for this compositional stratification to be preserved so well on a deposit scale, the magma chamber must not have experienced significant syn-eruptive mixing, and equally convection within the magma chamber must have had relatively little influence on the stratification, once crystals were forming, in order to preserve the zoning within the magma chamber.

It seems likely that no chamber-wide convection was occurring due to reasons discussed above, however this raises questions as to why convection was not occurring. We

1 see no evidence for a thermal stratification in the magma body, with no systematic

2 differences in modelled Fe–Ti oxide temperatures from the upper and lower regions of the

3 magma body. This does not negate the effect of crystallisation on the walls of the magma

4 chamber driving any convection, yet the relatively deep location of the storage region (~ 8.5

5 km, see above) compared to the depth to the Moho (~12 km; Klingelhöfer et al., 2001) and

6 the higher geothermal gradient in oceanic lithosphere may mean that this effect is minimal

7 when compared with magma storage zones on continents. However, given the lack of

8 evidence for new magmatic influx into the storage region, there will be a finite time period

9 over which the stored magma remains in an eruptible state. Lack of convective heat loss and

10 latent heat of crystallisation will maintain eruptive temperature (e.g. Karlstrom et al., 2009)

11 and counteract the conductive heat loss to the surrounding lithosphere. Estimation of the

12 maximum timescales for residence would require better knowledge of the chamber volume

13 and geometry than is provided by the erupted deposits. However, we would suggest that the

14 eruptive window (the timescale over which a magma remains in an 'eruptible state') must be

15 comparatively short, in the absence of any influx of new, hotter material. Available field

16 evidence (rapid attenuation in deposit thickness over distances) would suggest that the

17 erupted volume was comparatively small.

18

19 *Eruptive triggers*

20 Understanding the triggering mechanisms of volcanic eruptions is vital for monitoring active

21 volcanoes and forecasting future activity. Commonly cited triggers range from internal

22 triggers due to overpressure from volatile oversaturation or magmatic intrusion (e.g. Jellinek

23 & DePaolo, 2003; Caricchi et al., 2014) or magma mixing driving catastrophic destabilisation

24 of the magmatic system (e.g. Saunders et al., 2012; Albino and Sigmundsson, 2014; Till et

25 al., 2015). External triggers, outside of the magmatic system include tectonic activity (e.g.

26 Allan et al., 2012) or changing stress-state (e.g. Bonali et al., 2013).

27   One of the more commonly citerd eruptive triggers is magma maixing, yet there is no

28 evidence for magma mixing preserved in the pumice or scoria clasts of the zoned fall deposit

29 and magma evolution appears to have occurred in a closed-system with no subsequent

30 perturbation of the system (Fig. 6 – 8). The apparently low magmatic flux, when compared

31 with other ocean islands such as Iceland, Hawaii and the Canary Islands, may have allowed

32 the magma responsible for the zoned fall to remain isolated from other magmatic pulses (cf.

33 Sverisdottir, 2007; Albert et al., 2016). Therefore magma mixing was not an eruptive trigger

34 for the eruption of the zoned fall.

1   Another potential eruptive trigger is tectonic activity. Ascension Island's location

2   within 100 km of the MAR, and within 50 km of the AFZ, means that there will be

3   earthquakes of magnitudes greater than 4 in the region, which could affect magma chamber

4   stability (Manga and Brodsky et al., 2006). No direct evidence is preserved in the crystal or

5   melt compositions to link the eruption of the zoned fall to any regional tectonic activity; with

6   all phases being in apparent equilibrium with their surrounding melt. Magmatic evolution

7   appears to have proceeded in a relatively stable tectonic environment (see Evolution of zoned

8   fall section above). Yet, we cannot preclude earthquake activity as an eruptive trigger, that

9   left no record in the crystal cargo (cf. Allan et al., 2012).

10   Internal overpressure within a closed system is another potential eruptive trigger,

11 where crystal fractionation increases the concentration of magmatic volatiles in the magma

12 (cf. Tait et al., 1989). The high H_2O contents measured in melt inclusions (up to 4 wt%), and

13 well-understood role of closed-system evolution of the zoned fall make this the most

14 plausible eruptive trigger, as H_2O has the greatest effect in generating overpressures in

15 magma, due to its more soluble nature (Tait et al., 1989, Stock et al., 2016). Therefore, the

16 eruption of the zoned fall appears to have been primed by increasing internal

17 overpressurisation due to volatile oversaturation. However, while volatile oversaturation

18 undoubtedly primed the magma body for eruption, the trigger may have been a combination

19 of factors, including local earthquake activity, of which no record is preserved.

20

21 *Generation of silicic magmas at Ascension Island*

22 The zoned fall deposit is only one of multiple felsic explosive deposits on Ascension Island,

23 in its ~ 1 Myr subaerial history (Kar et al., 1998; Hobson, 2001; Jicha et al., 2014). Previous

24 work has investigated the origins of evolved magmas on Ascension Island (Kar et al., 1998),

25 and there has been only minor petrological investigation of eruptions (generally only the

26 evolved lavas: Harris 1983) and none has benefitted from a well-established volcanic

27 stratigraphy, or precise eruption dates, to be able to test if magmatic processes and timescales

28 vary with time on Ascension Island. Previous work has suggested varying importance for the

29 roles of both fractional crystallisation and assimilation (see Kar et al., 1998; Weaver et al.,

30 1998; Webster & Rebbert, 2001), with some older work even suggesting the presence of a

31 single large magma chamber feeding Ascension Island silicic volcanism (Kar et al., 1998). In

32 this instance, it is clear that fractional crystallisation and minor amounts of crystal

33 accumulation in a relatively closed magmatic system is responsible for the generation of the

34 compositional zonation preserved in the studied fall deposit. It is interesting to note that the

difference between most- and least-evolved compositions sampled by the zoned fall deposit is not large (54.5 wt.% SiO_2 at the top of the deposit to 60.5 wt.% SiO_2 at the deposit base; Fig. 5 and Electronic Appendix)- it is possible that all pumice fall deposits on Ascension Island are compositionally zoned, but did not cross the pumice-scoria textural boundary, and thus appear unzoned in the field. Further work is required to test for zonation in any of the other explosive silicic deposits.

The generally closed-system evolution of the zoned fall makes Ascension Island appear anomalous when compared with other classic ocean island volcanoes such as Hawaii, Iceland and the Canaries (see above). Similarly, the zoned fall appears anomalous in that there is only evidence for a single stage of evolution in both the melt inclusions and crystal cargos examined. This contrasts with many other ocean islands that preserve evidence for polybaric fractionation (for example Tenerife: Sliwinski et al., 2015; Iceland: Mancini et al., 2015; the Azores: Genske et al., 2012). It seems unlikely that the less-evolved end-member of the zoned fall deposit is a parental magma for Ascension, due to its generally more-evolved composition than many other Ascension lavas (see grey shaded area on Fig. 5a). Therefore this magma must have differentiated prior to evolution within the zoned fall magma reservoir. That this stage is not preserved in any crystals present in the zoned fall implies effective liquid-crystal separation at an earlier stage of evolution, potentially feasible due to the lower viscosity of the alkaline magmas at Ascension.

CONCLUSIONS

By studying the zoned fall deposit on Ascension Island we have garnered significant insights into the generation of this deposit, but have also raised questions regarding the generation and evolution of silicic magmas at Ascension Island and other ocean island volcanoes. Our main conclusions are summarised below:

1. A unique zoned fall deposit on Ascension Island displays a systematic gradation in composition, grading from trachyte at the base, to trachy-basaltic andesite at the top of the deposit. This zonation results from the evacuation of a single compositionally (but not thermally) zoned magma batch residing at ~8.5 km depth: the base of oceanic crust at Ascension.

2. The zonation within the magma body occurred through closed-system crystal fractionation of mainly feldspar and olivine, with minor amounts of clinopyroxene, Fe–Ti oxides and apatite, and the accumulation of a sanidine-anorthoclase feldspar phase, likely to be from older plutonic bodies present in the crust. This relatively

simple evolutionary path for the generation of evolved magmas in thin oceanic lithosphere at Ascension contrasts with many other ocean island volcanoes, where magma supply rates are higher and therefore favour more complex magmatic interactions and open system behaviour.

3. The eruption of the zoned fall deposit appears to have been internally triggered, via fractional crystallisation concentrating volatiles into the melt phase, and eventually leading to over-pressurisation. This is supported by the high volatile content melt inclusions; the lack of any hydrous crystal phases that could accommodate increased H_2O concentrations; and the lack of evidence for magma mixing. While there is no geochemical evidence for tectonics triggering the eruption of the zoned fall deposit (cf. Allan et al., 2012), this may not be recorded in the crystal cargo, and thus a tectonic role in the eruption of the zoned fall cannot be precluded.

4. The data show a lack of apparent coupling between reducing oxygen fugacities in the zoned fall on Ascension Island (fO$_2$ ~ -2.2 log units ΔNNO) and elevated H_2O contents (up to 4 wt.% H_2O) similar to that observed by Portnyagin et al. (2012) in Iceland. Thus, while the source of Ascension Island magmas may be reducing (and therefore impart a reduced oxygen fugacity on the magma) this is not affected by evolution and fractionation. Yet, due to the absence of hydrous crystal phases on Ascension Island, H_2O contents increase in the magma body with increasing degrees of evolution, yielding water-rich erupted magma compositions.

5. The zonation preserved in the zoned fall deposit on Ascension, highlighted by the textural change from pumice at the base to scoria at the top of the deposit, may be present in other fall deposits on Ascension, whose composition does not cross the pumice-scoria textural boundary. Further work is needed to assess how applicable the magmatic processes responsible outlined here are to all silicic volcanism on Ascension Island.

REFERENCES

Ablay, G. J., Carroll, M. R., Palmer, M. R., Martí, J., & Sparks, R. S. J. (1998). Basanite–phonolite lineages of the Teide–Pico Viejo volcanic complex, Tenerife, Canary Islands. *Journal of Petrology*, *39*(5), 905-936.

Albert, H., Costa, F., & Martí, J. (2016). Years to weeks of seismic unrest and magmatic intrusions precede monogenetic eruptions. *Geology*, *44*(3), 211-214.

Albino, F., & Sigmundsson, F. (2014). Stress transfer between magma bodies: Influence of intrusions prior to 2010 eruptions at Eyjafjallajökull volcano, Iceland. *Journal of Geophysical Research: Solid Earth*, *119*(4), 2964-2975.

Allan, A. S., Wilson, C. J., Millet, M. A., & Wysoczanski, R. J. (2012). The invisible hand: tectonic triggering and modulation of a rhyolitic supereruption. *Geology*, *40*(6), 563-566.

Bacon, C. R. & Hirschmann, M. M. (1988). Mg/Mn partitioning as a test for equilibrium between coexisting Fe^Ti oxides. *American Mineralogist 73,* 57-61

Blundy, J., & Cashman, K. (2008). Petrologic reconstruction of magmatic system variables and processes. *Reviews in Mineralogy and Geochemistry*, *69*(1), 179-239.

Bonadonna, C., Cioni, R., Pistolesi, M., Connor, C., Scollo, S., Pioli, L., & Rosi, M. (2013). Determination of the largest clast sizes of tephra deposits for the characterization of explosive eruptions: a study of the IAVCEI commission on tephra hazard modelling. *Bulletin of volcanology*, *75*(1), 1-15.

Bonali, F. L., Tibaldi, A., Corazzato, C., Tormey, D. R., & Lara, L. E. (2013). Quantifying the effect of large earthquakes in promoting eruptions due to stress changes on magma pathway: the Chile case. *Tectonophysics*, *583*, 54-67.

Caricchi, L., Annen, C., Blundy, J., Simpson, G. & Pinel, V. (2014). Frequency and magnitude of volcanic eruptions controlled by magma injection and buoyancy. *Nature Geoscience 7*, 126–130.

Carley, T. L., Miller, C. F., Wooden, J. L., Bindeman, I. N., & Barth, A. P. (2011). Zircon from historic eruptions in Iceland: reconstructing storage and evolution of silicic magmas. *Mineralogy and Petrology*, *102*(1-4), 135-161.

Carmichael, I. S. (1991). The redox states of basic and silicic magmas: a reflection of their source regions? *Contributions to Mineralogy and Petrology*, *106*(2), 129-141.

Daly, R. A. (1925, June). The geology of Ascension island. In *Proceedings of the American Academy of Arts and Sciences* (Vol. 60, No. 1, pp. 3-80). American Academy of Arts & Sciences.

Gazel, E., Hayes, J. L., Kelemen, P. B., Everson, E. D., Holbrook, W. S., & Vance, E. (2014, December). Generation of continental crust in intra-oceanic arcs. In *AGU Fall Meeting Abstracts* (Vol. 1, p. 4845).

Genske, F. S., Turner, S. P., Beier, C., & Schaefer, B. F. (2012). The petrology and geochemistry of lavas from the western Azores islands of Flores and Corvo. *Journal of Petrology*, *53*(8), 1673-1708.

Ghiorso, M. S., & Evans, B. W. (2008). Thermodynamics of rhombohedral oxide solid solutions and a revision of the Fe-Ti two-oxide geothermometer and oxygen-barometer. *American Journal of Science*, *308*(9), 957-1039.

Gualda, G. A., & Ghiorso, M. S. (2014). Phase-equilibrium geobarometers for silicic rocks based on rhyolite-MELTS. Part 1: Principles, procedures, and evaluation of the method. *Contributions to Mineralogy and Petrology*, *168*(1), 1-17.

Harris, C. (1983). The petrology of lavas and associated plutonic inclusions of Ascension Island. *Journal of Petrology*, *24*(4), 424-470.

Hobson, K.E. (2001). The pyroclastic deposits and eruption history of Ascension Island: a palaeomagnetic and volcanological study. *Doctoral dissertation, University of Oxford*.

Humphreys, M., Kearns, S.L. and Blundy, J.D., 2006. SIMS investigation of electron-beam damage to hydrous, rhyolitic glasses: Implications for melt inclusion analysis. *American Mineralogist*, *91*(4), 667-679.

Jellinek, A. M., & DePaolo, D. J. (2003). A model for the origin of large silicic magma chambers: precursors of caldera-forming eruptions. *Bulletin of Volcanology*, *65*(5), 363-381.

Jicha, B. R., Singer, B. S., & Valentine, M. J. (2013). 40Ar/39Ar Geochronology of Subaerial Ascension Island and a Re-evaluation of the Temporal Progression of Basaltic to Rhyolitic Volcanism. *Journal of Petrology*, *54*(12), 2581-2596.

Kar, A., Weaver, B., Davidson, J., & Colucci, M. (1998). Origin of differentiated volcanic and plutonic rocks from Ascension Island, South Atlantic Ocean. *Journal of Petrology*, *39*(5), 1009-1024.

Karlstrom, L., Dufek, J., & Manga, M. (2009). Organization of volcanic plumbing through magmatic lensing by magma chambers and volcanic loads. *Journal of Geophysical Research: Solid Earth*, *114*(B10).

Klingelhöfer, F., Minshull, T. A., Blackman, D. K., Harben, P., & Childers, V. (2001). Crustal structure of Ascension Island from wide-angle seismic data: implications for the formation of near-ridge volcanic islands. *Earth and Planetary Science Letters*, *190*(1), 41-56.

Kuritani, T., Yokoyama, T., Kitagawa, H., Kobayashi, K., & Nakamura, E. (2011). Geochemical evolution of historical lavas from Askja Volcano, Iceland: Implications for mechanisms and timescales of magmatic differentiation. *Geochimica et Cosmochimica Acta*, *75*(2), 570-587.

Lee, C. T. A., Leeman, W. P., Canil, D., & Li, Z. X. A. (2005). Similar V/Sc systematics in MORB and arc basalts: implications for the oxygen fugacities of their mantle source regions. *Journal of Petrology*, *46*(11), 2313-2336.

Malfait, W.J., Seifert, R., Petitgirard, S., Perrillat, J.P., Mezouar, M., Ota, T., Nakamura, E., Lerch, P. and Sanchez-Valle, C., 2014. Supervolcano eruptions driven by melt buoyancy in large silicic magma chambers. *Nature Geoscience*, *7*(2), 122-125.

Mancini, A., Mattsson, H. B., & Bachmann, O. (2015). Origin of the compositional diversity in the basalt-to-dacite series erupted along the Heiðarsporður ridge, NE Iceland. *Journal of Volcanology and Geothermal Research*, *301*, 116-127.

Manga, M. and Brodsky, E., 2006. Seismic triggering of eruptions in the far field: volcanoes and geysers. *Annu. Rev. Earth Planet. Sci*, *34*, 263-291.

Minshull, T. A., Ishizuka, O., & Garcia-Castellanos, D. (2010). Long-term growth and subsidence of Ascension Island: Constraints on the rheology of young oceanic lithosphere. *Geophysical Research Letters*, *37*(23).

Morgan, D. J., Blake, S., Rogers, N. W., DeVivo, B., Rolandi, G., Macdonald, R., & Hawkesworth, C. J. (2004). Time scales of crystal residence and magma chamber volume from modelling of diffusion profiles in phenocrysts: Vesuvius 1944. *Earth and Planetary Science Letters*, *222*(3), 933-946.

Mortensen, A. K., Wilson, J. R., & Holm, P. M. (2009). The Cão Grande phonolitic fall deposit on Santo Antão, Cape Verde Islands. *Journal of Volcanology and Geothermal Research*, *179*(1), 120-132.

Nielson, D. L., & Sibbett, B. S. (1996). Geology of Ascension Island, South Atlantic Ocean. *Geothermics*, *25*(4), 427-448.

Nielson, D. L., Adams, M. C., Sibbett, B. S., & Wright, P. M. (1996). Shallow thermal structure and hydrology of Ascension Island, south Atlantic Ocean. *Geothermics*, *25*(4), 521-541.

Pallister, J. S., Hoblitt, R. P., & Reyes, A. G. (1992). A basalt trigger for the 1991 eruptions of Pinatubo Volcano? *Nature,* 356, 426-428.

Petrelli, M., Poli, G., Perugini, D., & Peccerillo, A. (2005). PetroGraph: A new software to visualize, model, and present geochemical data in igneous petrology. *Geochemistry, Geophysics, Geosystems*, *6*(7).

Portnyagin, M., Hoernle, K., Storm, S., Mironov, N., van den Bogaard, C., & Botcharnikov, R. (2012). H 2 O-rich melt inclusions in fayalitic olivine from Hekla volcano: implications for phase relationships in silicic systems and driving forces of explosive volcanism on Iceland. *Earth and Planetary Science Letters*, *357*, 337-346.

Saunders, K., Blundy, J., Dohmen, R., & Cashman, K. (2012). Linking petrology and seismology at an active volcano. *Science*, *336*(6084), 1023-1027.

Sharp, W. D., & Renne, P. R. (2005). The 40Ar/39Ar dating of core recovered by the Hawaii Scientific Drilling Project (phase 2), Hilo, Hawaii. *Geochemistry, Geophysics, Geosystems*, *6*(4).

Sliwinski, J. T., Bachmann, O., Ellis, B. S., Dávila-Harris, P., Nelson, B. K., & Dufek, J. (2015). Eruption of Shallow Crystal Cumulates during Explosive Phonolitic Eruptions on Tenerife, Canary Islands. *Journal of Petrology*, egv068.

Snyder, D., 2000. Thermal effects of the intrusion of basaltic magma into a more silicic magma chamber and implications for eruption triggering. *Earth and Planetary Science Letters*, *175*(3), 257-273.

Snyder, D. C., Widom, E., Pietruszka, A. J., Carlson, R. W., & Schmincke, H. U. (2007). Time scales of formation of zoned magma chambers: U-series disequilibria in the Fogo A and 1563 AD trachyte deposits, São Miguel, Azores. *Chemical geology*, *239*(1), 138-155.

Sparks, S.R. & Sigurdsson, H., 1977. Magma mixing: a mechanism for triggering acid explosive eruptions. *Nature*, *267*, 315-318.

Stock, M.J., Humphreys, M.C., Smith, V.C., Isaia, R. and Pyle, D.M., 2016. Late-stage volatile saturation as a potential trigger for explosive volcanic eruptions. *Nature Geoscience*, *9*(3), 249-254.

Stormer, J. C., & Nicholls, J. (1978). XLFRAC: a program for the interactive testing of magmatic differentiation models. *Computers & Geosciences*, *4*(2), 143-159.

Sverrisdottir, G. (2007). Hybrid magma generation preceding Plinian silicic eruptions at Hekla, Iceland: evidence from mineralogy and chemistry of two zoned deposits. *Geological Magazine*, *144*(04), 643-659.

Tait, S., Jaupart, C., & Vergniolle, S. (1989). Pressure, gas content and eruption periodicity of a shallow, crystallising magma chamber. *Earth and Planetary Science Letters*, *92*(1), 107-123.

Till, C. B., Vazquez, J. A., & Boyce, J. W. (2015). Months between rejuvenation and volcanic eruption at Yellowstone caldera, Wyoming. *Geology*, *43*(8), 695-698.

Walker, G. P. (1966). Acid volcanic rocks in Iceland. *Bulletin Volcanologique*, *29*(1), 375-402.

Watanabe, S., Widom, E., Ui, T., Miyaji, N., & Roberts, A. M. (2006). The evolution of a chemically zoned magma chamber: The 1707 eruption of Fuji volcano, Japan. *Journal of volcanology and geothermal research*, *152*(1), 1-19.

Weaver, B., Kar, A., Davidson, J., & Colucci, M. (1996). Geochemical characteristics of volcanic rocks from Ascension Island, south Atlantic Ocean. *Geothermics*, *25*(4), 449-470.

Webster, J. D., & Rebbert, C. R. (2001). The geochemical signature of fluid-saturated magma determined from silicate melt inclusions in Ascension Island granite xenoliths. *Geochimica et Cosmochimica Acta*, *65*(1), 123-136.

Wiesmaier, S., Troll, V. R., Wolff, J. A., & Carracedo, J. C. (2013). Open-system processes in the differentiation of mafic magma in the Teide–Pico Viejo succession, Tenerife. *Journal of the Geological Society*, *170*(3), 557-570.
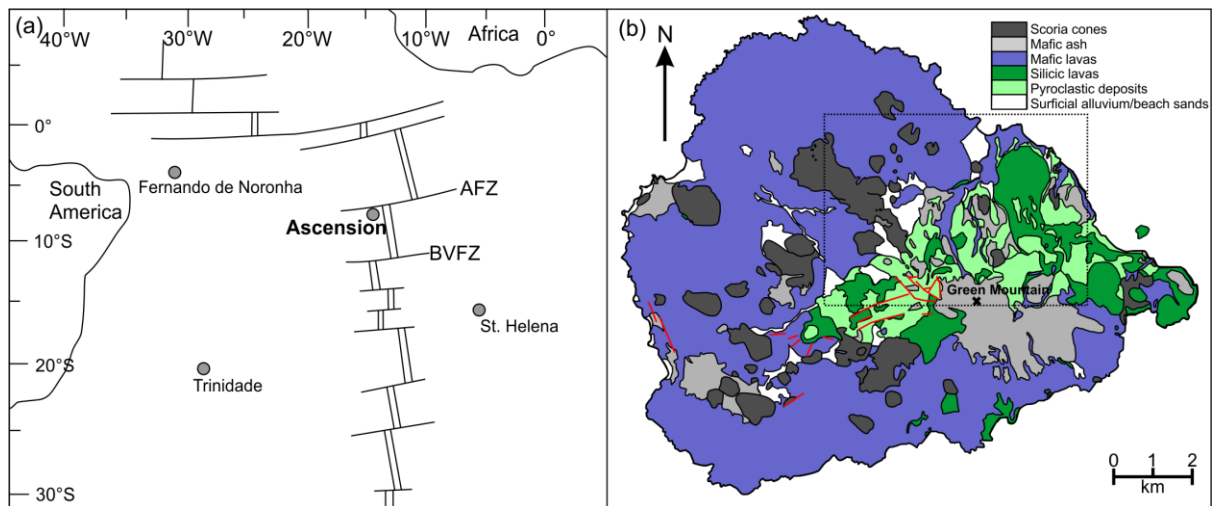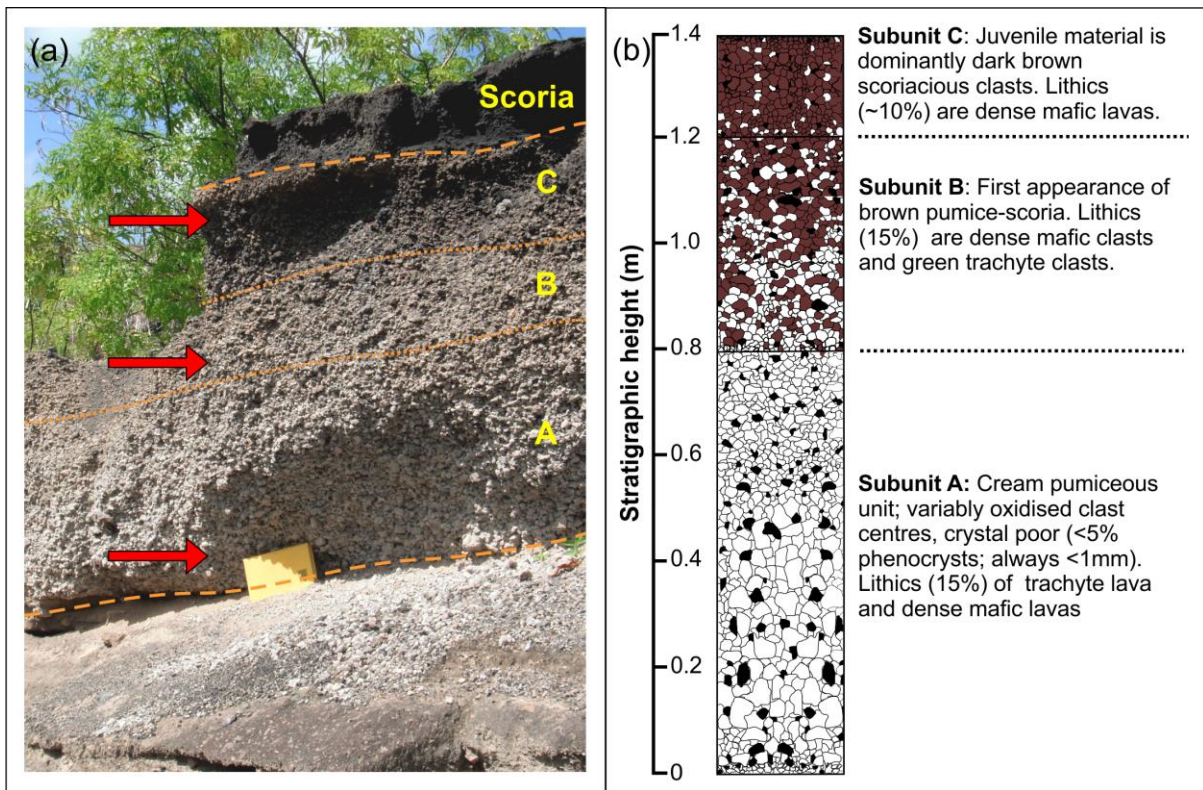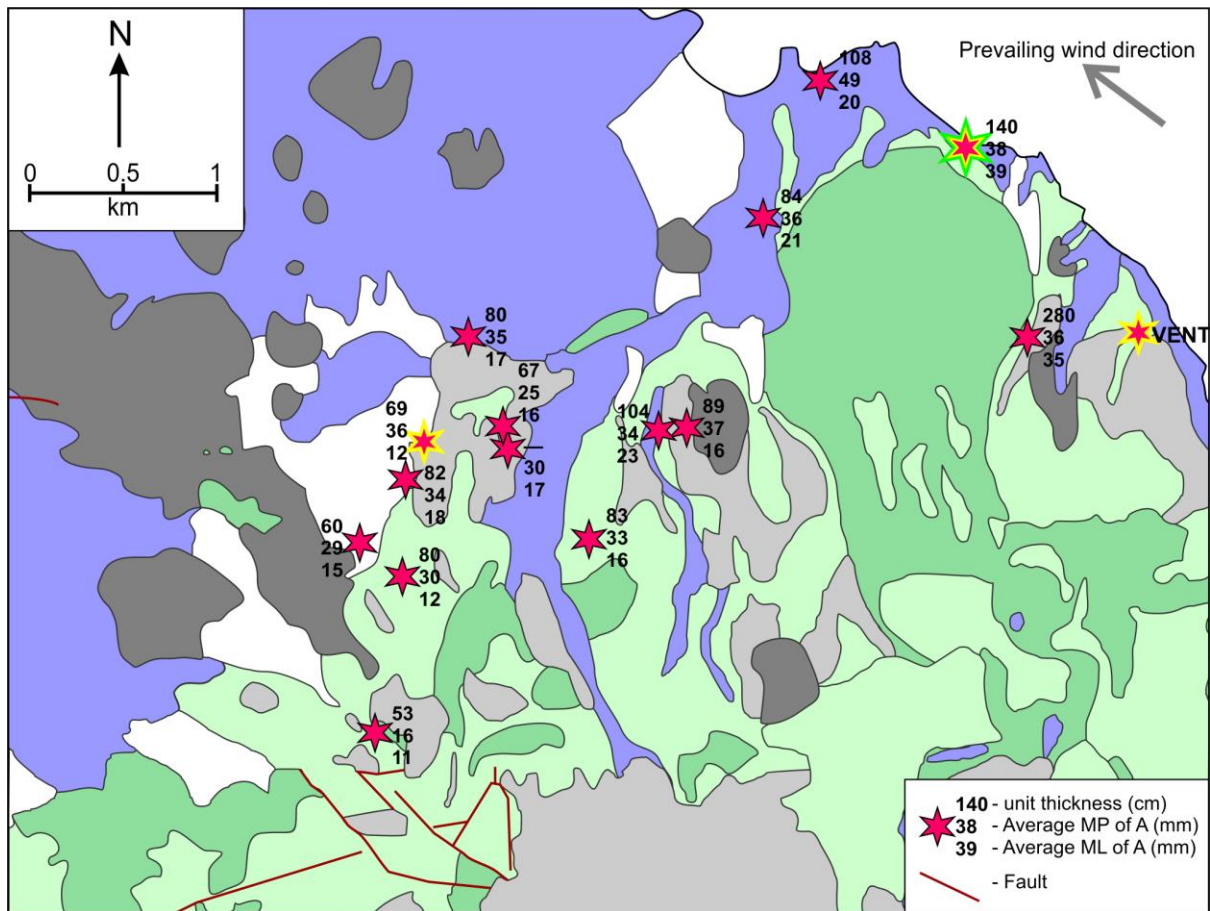
1 **FIGURES**

2

3 Figure 1: Ascension Island location map (a) shown in relation to the Mid Atlantic Ridge, the

4 Ascension Fracture Zone (AFZ) and the Bode Verde Fracture Zone (BVFZ). Geological map

5 of Ascension Island (b) showing the areas where lavas, scoria cones and pyroclastic deposits

6 are exposed at the surface. Faults are shown as red lines.

1

2
3 Figure 2: Zoned fall deposit of Ascension Island. (a) The compositionally zoned fall at
4 showing the three transitional subunits A to C, and the overlying scoria. Notebook is 205 mm
5 wide for scale. Representative stratigraphic log through the zoned fall along with subunit
6 descriptions (b). Lithic clasts are shown as black clasts, with pumice as white clasts and
7 scoria as brown clasts. Colour of juvenile clasts relates only to their textural association,
8 rather than retaining any compositional information, or reflecting the colours of the juvenile
9 clasts in the subunits. Clasts shown to scale.

Figure 3: Zoned fall localities (pink stars) overlain over the geological map of Ascension (area shown in Fig. 1). The numbers for the zoned fall outcrops indicate total unit thickness in cm, the geometric mean of the 5 largest pumice dimension in subunit A, in mm (following Bonadonna et al., 2013) and the geometric mean of the 5 largest lithic clasts in A, in mm (following Bonadonna et al., 2013). Where no thickness is given, the full sequence of the unit has not been preserved. Locations where samples were collected are outlined in yellow, with the unit outlined in yellow and green being the location where all samples of subunits A, B and C analysed for melt inclusions were collected.
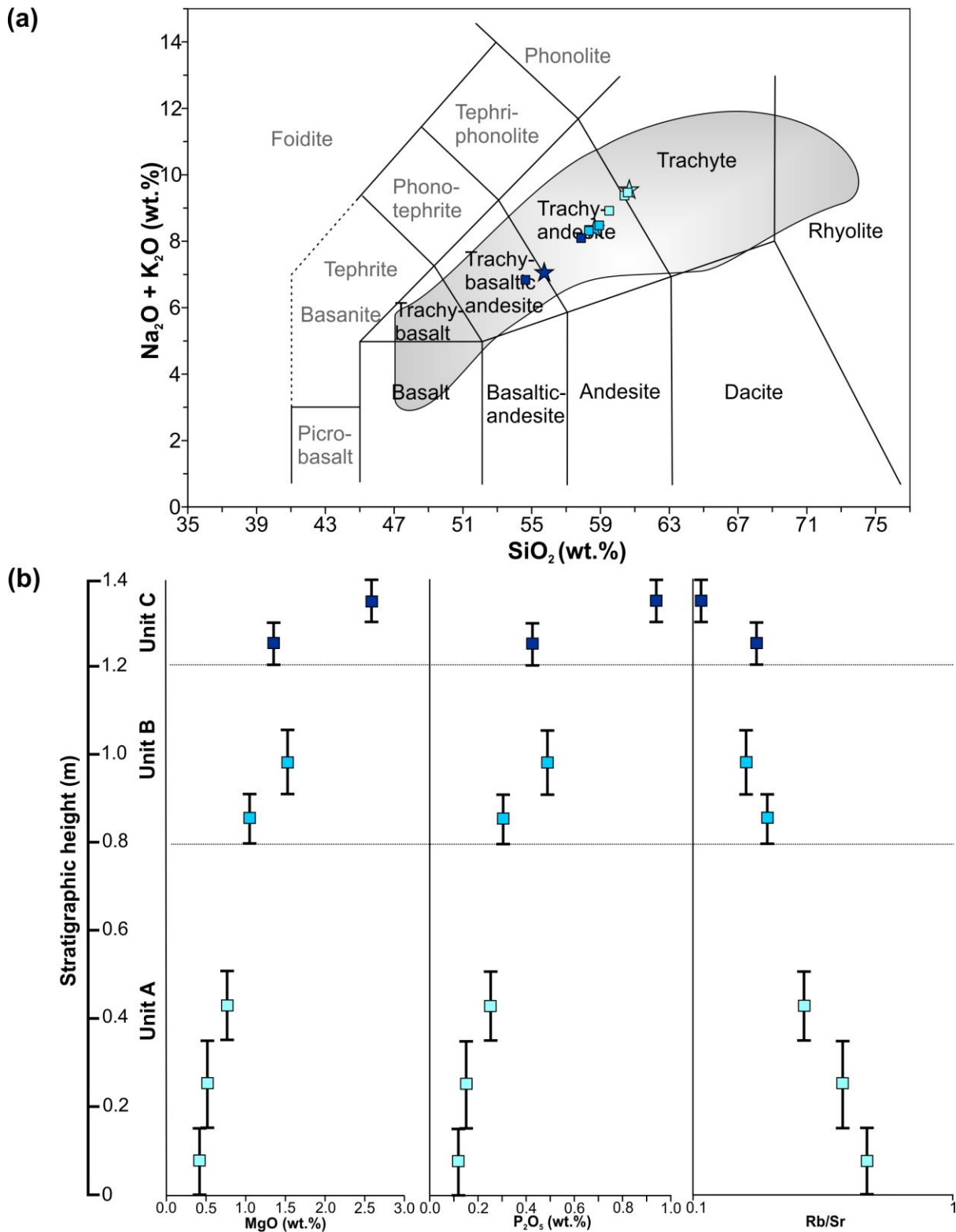
1
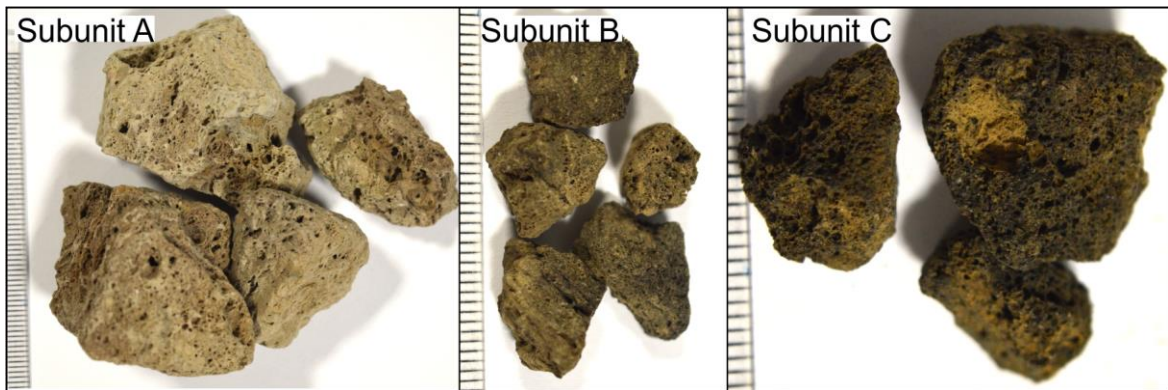
3   Figure 4: Juvenile clasts from the 3 subunits of the zoned fall deposit from pumice in subunit
4   A, through to scoria in subunit C. Scale dashes are in 1 mm intervals, for reference.

2

Figure 5: Whole-rock geochemical data from samples at selected stratigraphic heights within
the identified subunits (labelled). (a) Total Alkalis-Silica plot for all samples listed in Table 1
(for full data set see Electronic Appendix). Stars indicate bulk samples of subunits (A being
lightest blue, B middle blue, C darkest blue). Squares are samples within these units, colour

1   coded by subunit they belong to. (b) shows selected elements changing with stratigraphic

2   height. Black bars indicate the thickness of the region sampled for each whole rock analysis.
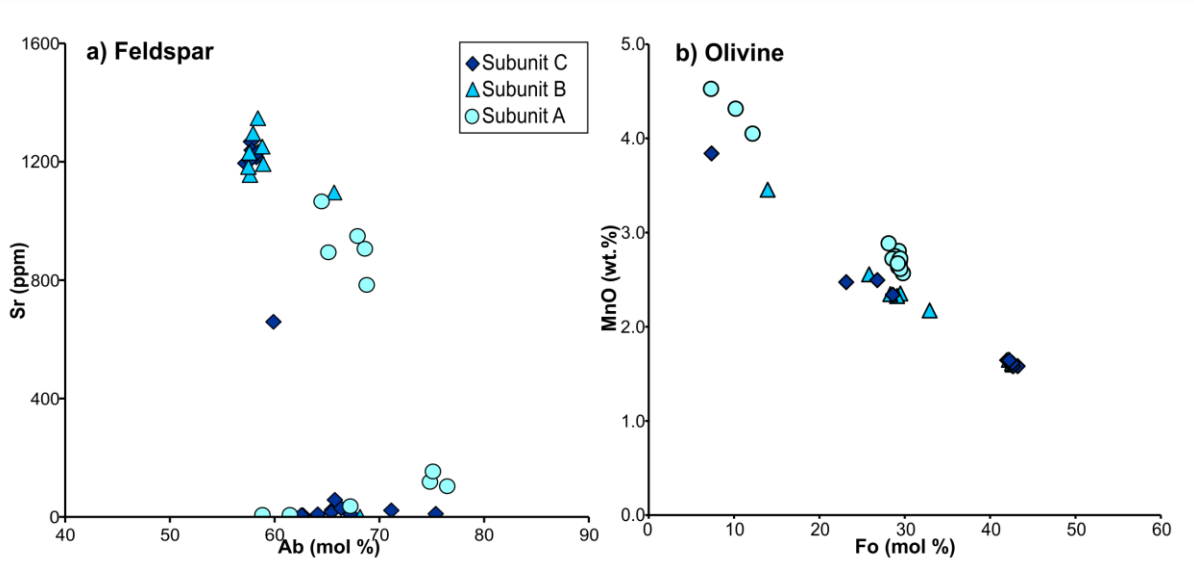
3

4

5
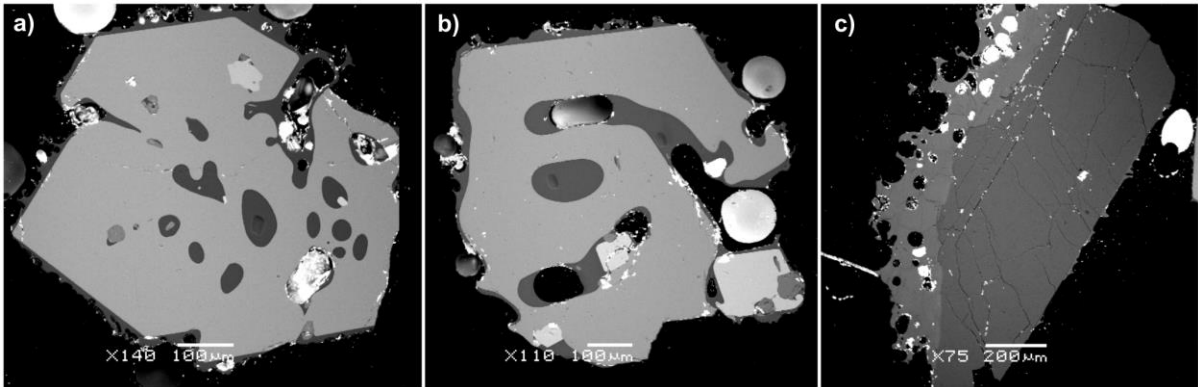
6

7   Figure 6: Back scattered electron (BSE) images of representative crystals from subunits A –

8   C. No zoning is evident in either the melt inclusion-bearing olivine (a), (b) or the feldspar (c).

9   SIMS spot locations for melt inclusion analyses are evident in (a) and (b). In (a) and (b) the

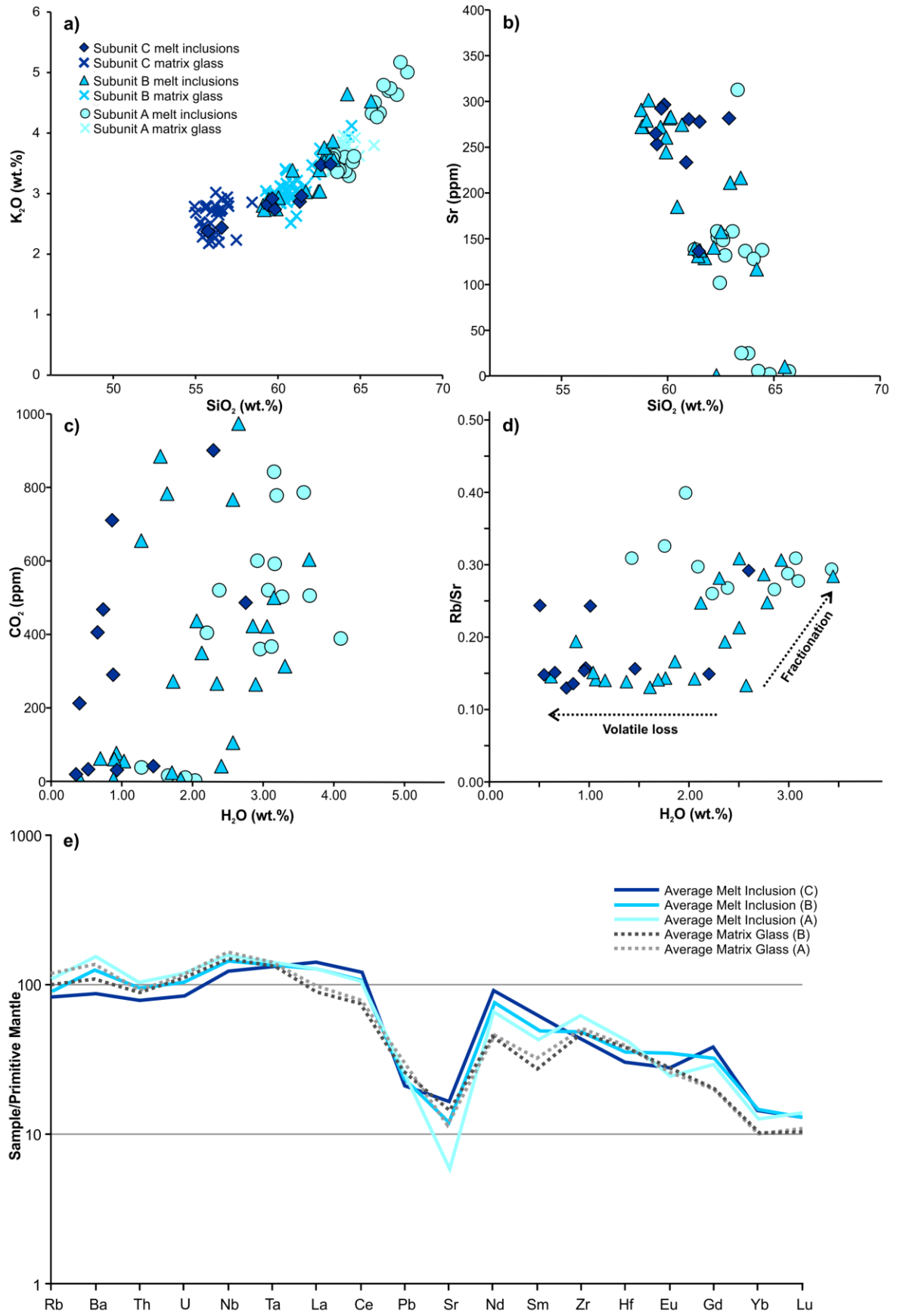10   scale bar in 100 μm, in (c) the scale bar is 200 μm.

11

1

Figure 7: Phenocryst compositions of feldspar (a) and olivine (b) from the three major subunits identified. Subunit A (circles), subunit B (triangles) and subunit C (squares). For all data see Electronic Appendix.

1

1 Figure 8: (a) Matrix glass (crosses) and melt inclusion (filled symbols) compositions from the

2 three main subunits of the zoned fall. (b-d) melt inclusion compositions and volatile

3 concentrations from all three main subunits of the zoned fall; subunit symbols as in previous

4 figure. (e) Primitive mantle normalised (Sun & McDonough, 1985) trace element diagrams

5 for average matrix glass (dashed) and melt inclusion (solid lines) compositions from the three

6 major subunits. No matrix glass trace element data available for subunit C due to the coarsely

7 microcrystalline nature of the groundmass. Colours as in previous figures. For all data see
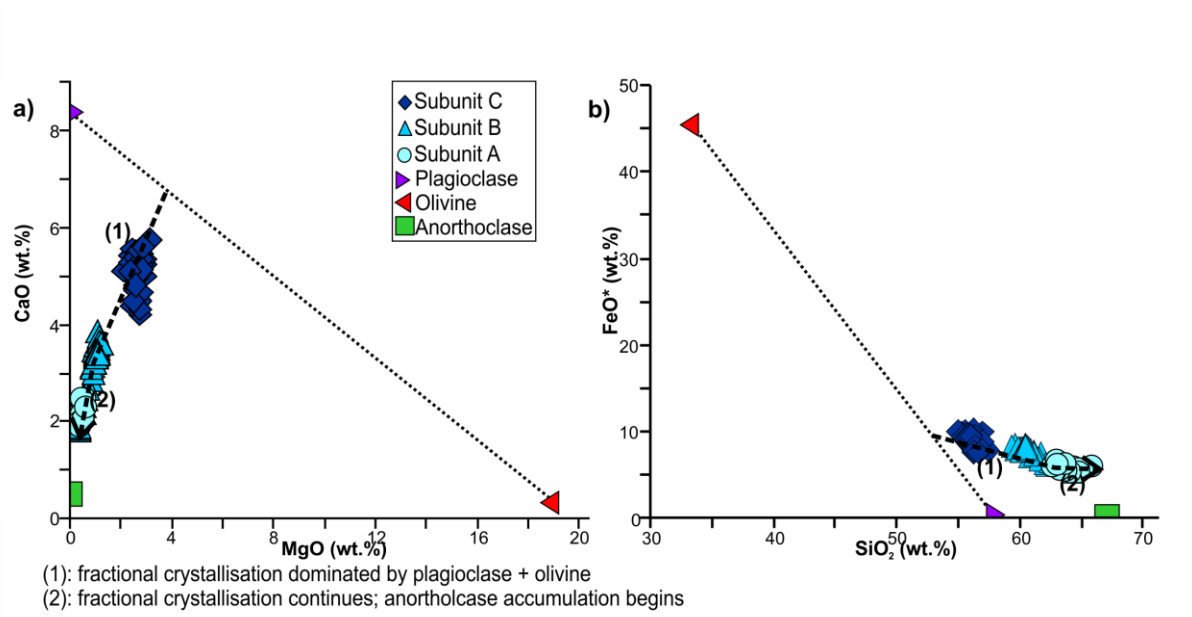
8 Electronic Appendix.

9

1
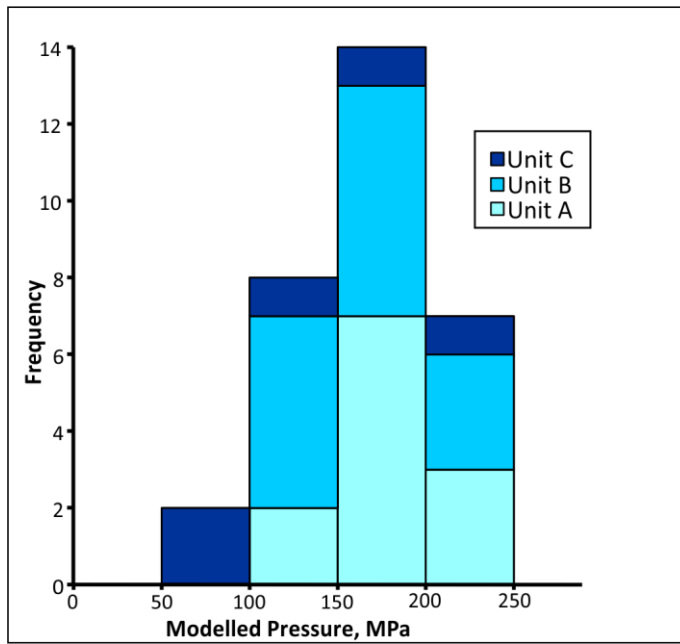
2

3 Figure 9: Histogram of modelled entrapment pressures (using MagmaSat of Ghiorso &

4 Gualda, 2015) for melt inclusions from all three subunits (colours in previous figures) of the

5 zoned fall. For all data see Electronic Appendix.

6

1

Figure 10: Matrix glass compositions compared with the compositions of the three dominant crystal phases; subunit symbols as in previous figure. Stage 1 shows fractional crystallisation of plagioclase feldspar and olivine driving the evolution of the matrix glass. Stage 2 highlights the influence of the accumulation of anorthoclase feldspar. Compositions of crystal phases are average compositions from subunit C (plagioclase and olivine), and subunit B (anorthoclase feldspar). For all data see Electronic Appendix.

9

1   **Table 1:** Samples of the compositionally-zoned fall

Sample	Stratigraphic height sampled over (in cm from base)	Subunit
AI15-628A	Bulk sample 0 – 80cm	A
AI14-439G	0 – 15cm	A
AI14-439F	15 – 35cm	A
AI14-439E	35 – 50cm	A
AI15-628B	Bulk sample 80 – 120cm	B
AI14-439D	80 – 90cm	B
AI14-439C	90 – 105cm	B
AI14-439B	120 – 130cm	C
AI14-439A	130 – 140cm	C
AI15-628C	Bulk sample 120 – 140cm	C

2

1 **Table 2:** Temperatures and entrapment pressures of the subunits of the compositionally-

2 zoned fall

Sample	Description	Average calculated Fe-Ti Oxide temperature [1] *(range)*	Average calculated fO2 ΔNNO [1] *(range)*	Maximum modelled entrapment pressure [2]
AI15-628A	Subunit A- lower	*845 °C* *(841 – 853)*	**-2.28** *(-2.30 – -2.26)*	**250 MPa**
AI15-628B	Subunit B- mid			**240 MPa**
AI15-628C	Subunit C- upper	**866 °C** *(819 – 886)*	**-1.94** *(-2.42– -1.83)*	**216 MPa**

3

4 (1) Using Ghiorso & Evans (2008) calibration
5 (2) Using the MagmaSat App developed from Gualda & Ghiorso (2014)
6